Braz J Phys (2015) 45:719–729
DOI 10.1007/s13538-015-0371-6

STATISTICAL

Dynamics Solved by the Three-Point Formula: Exact Analytical Results for Rings

Mircea Galiceanu[1,2] · Aurel Jurjiu[3] · Antonio Volta[4,5] · Marco Bittelli[4]

Received: 31 July 2015 / Published online: 28 September 2015

Abstract In this paper, we study in the framework of the Gaussian model, the relaxation dynamics, and diffusion process on structures which show a ring-shape geometry. In order to extend the classical connectivity matrix to include interactions between more distant nearest neighbors, we treat the second derivative with respect to position by using the three-point formula. For this new Laplacian matrix, we determine analytical solutions to the eigenvalue problem. The relaxation dynamics is described by the mechanical relaxation moduli and for diffusion we focus on the behavior of the residual concentration at the initial node. Additionally, we investigate the scaling behaviors of the mean squared radius of gyration and of the smallest eigenvalue. To calculate the residual concentration, we consider that initially the whole material is concentrated only in one node and then it spreads over the ring. We compare our results with the ones obtained from the incremental ratio method. We observe that the results of the two methods for the considered quantities are slightly different. At any intermediate time/frequency domain, the results obtained by using the incremental ratio method underestimate the ones obtained by using the three-point formula. This finding can turn important for many applications in polymer systems or in other systems where diffusive motion occurs.

Keywords Diffusion equation · Three-point formula · Eigenvalue problem · Residual concentration · Viscoelastic relaxation

1 Introduction

In the analysis of polymer dynamics, one of the central question is in which way the observed diffusion patterns and the mechanical response relate to the underlying geometry. This question has a long-standing history and is becoming of increased importance as new polymeric materials with more and more complex architectures are synthesized. Diffusion, starting from pioneering studies of the nineteenth century on, is one of utmost important topic in physics and more in general in science [1–5]. Diffusion on different types of structures was vastly explored in the last decades [6, 7]. In particular, this is a fundamental issue in systems with discrete structures like many of the polymer systems [8] and in systems where a continuum description must be reduced to discrete description in order to avoid cumbersome calculations. As an example for the last, in soil physics, the soil profile can be described through a finite volume approximation [9, 10] where the structure's nodes account for distinct portions of soil.

✉ Mircea Galiceanu
mircea@ufam.edu.br

Antonio Volta
antonio.volta@unibo.it

1 Departamento de Física, Universidade Federal do Amazonas, 69077-000 Manaus, Amazonas, Brazil

2 Institut für Theoretische Physik, Technische Universität Dresden, 01062 Dresden, Germany

3 Leibniz-Institut für Polymerforschung Dresden, e.V., Hohe Strasse 6, 01069 Dresden, Germany

4 Dipartimento di Scienze Agrarie, Università di Bologna, viale Fanin 44, 40127 Bologna, Italy

5 ARPA Emilia Romagna, Servizio Idro-Meteo-Clima, viale Silvani 6, 40122 Bologna, Italy

On discrete systems, the Laplacian operator adopts a matricial form which is described by the so called connectivity matrix $\mathbf{A_1}$ (index 1 to show that only the nearest neighbors interactions are considered). For a system consisting of N nodes, the connectivity matrix is an $N \times N$ real symmetric matrix, whose nondiagonal elements A_{ij} are -1 if the ith and jth nodes are directly connected with a bond and 0 otherwise; the diagonal elements A_{ii} equal the number of bonds emanating from the ith node. Matrices which describe connectivity are greatly used in different areas of physics. For instance, the Hückel matrix is used for determining the energy levels in PPP (MO) quantum calculations [11], the Kirchhoff matrix in the study of resistor networks, and the generalized Rouse matrix in the study of different properties of the polymers [12–15].

Gaussian models are extremely important because they allow one to treat the dynamical problem in the framework of linear algebra. In the Rouse-type approach, which assumes harmonic entropic forces between flexible nearest neighbors repeated units (monomers), many static and dynamic quantities (such as radius of gyration, mechanical relaxation moduli (storage and loss modulus), averaged monomer displacement, dielectric relaxation, residual concentration, probability to return to the origin) can be calculated based on the eigenvalue spectrum of the matrix structure describing the connectivity of the polymer. The Rouse model [16, 17] was developed for linear polymeric systems and for these systems, the eigenvalues of their connectivity matrices are determined analytically. The impact of monomer's connectivity on the physical properties of polymer structures leaded to the generalization of the Rouse approach to a model which includes structures with more complex geometries. In the literature, this model has obtained the more technical term generalized Gaussian structures or simply GGS [12–15, 17]. The GGS model has the same limitations, it does not account for the excluded volume constraints and for the entanglements effects, but, on the other hand, it allows one to explore very efficiently the structural properties, as well as the dynamical properties of arbitrarily connected polymer structures by making use of the eigenvalues of the connectivity matrix. Furthermore, the determination of the eigenvalues of the connectivity matrix through iterative or semi-analytical methods offers the possibility to investigate the dynamics of polymer structures consisting of huge number of monomers and at larger time scales than those accessible in computer simulations. To our knowledge, there are only few structures in the literature for which the eigenvalues of their connectivity matrices can be determined iteratively. These are the dendrimers [18, 19] and their dual structures called the Husimi cacti [20, 21], the dual Sierpinski gasket and its generalization to arbitrary dimension [22–24], the Vicsek fractals with every functionality (also with trap) [25–27], multihierarchical structure VFRSDSG [28], the multilayered structure based on Vicsek fractals [29], and special classes of small-world networks [30] and scale-free networks [31]. For all these mentioned structures, the connectivity matrices were built accounting only nearest neighbors interactions, i.e., $\mathbf{A_1}$. From the way of constructing the connectivity matrix in the Rouse case, where, as we said above, only the topological *connectivity* between nearest neighbors is considered meaning that a bond between nodes i and j is accounted for by incrementing the diagonal elements A_{ii} and A_{jj} by $+1$ and A_{ij} and A_{ji} the by -1, we call this method as the incremental ratio method.

To perform better approximations in evaluating derivatives, one can use n-points formulas. In this work, we study the mechanical relaxation and the diffusion on discrete rings (or circles) by applying the three-point formula [32]. With this method, we extend the classical Rouse connectivity matrix to incorporate interactions between other more distant neighbors. We determine the eigenvalue spectrum of the new Laplacian operator $\mathbf{A_3}$ (index 3 because of the three-point formula). Remarkably, for this matrix, which is also real symmetric, we succeeded to determine analytically its full eigenvalue spectrum and eigenvectors, thereby avoiding the numerical diagonalization. Based on the eigenvalues obtained in the iterative manner, we study the relaxation dynamics by focusing on the behavior of the mechanical relaxation moduli and the diffusion process by investigating the behavior of the residual concentration at the initial node of motion. We noticed readable differences between the results obtained by using the incremental ratio and the three-point formula at intermediate time or frequency domains, although scaling is present in both descriptions. Moreover, these different features clearly appear independent of the network size. Additionally, we also investigate the behaviors of the mean squared radius of gyration and of the smallest eigenvalue. The main purpose of the investigation of these additional quantities is to see if the scaling relations and the scaling exponents obtained in the Rouse-type approach are still preserved by the introduction of interactions between more distant neighbors. We observed a very good agreement between the theory and the approximations. The paper is structured as follows: In Section 2, we determine analytically the eigenvalue spectrum of $\mathbf{A_3}$ using the approximation for the second-order derivative obtained by implementing the three-point formula, which is described in Appendix A. We compare the spectrum of $\mathbf{A_3}$ with the $\mathbf{A_1}$ spectrum. In Section 3, we show the behavior of the residual concentration at the initial node with both techniques. In Section 4, we treat the relaxation dynamics by computing the components of the complex modulus. In Section 5, we show the results obtained for the mean squared radius of gyration and for the smallest eigenvalue. In Section 6, we resume the results and their implications.

2 Diffusion Equation on Rings

Our aim is to describe standard diffusion on a discrete 1D system with periodic boundary conditions, i.e., a ring consisting of N nodes. The problem of diffusion in discrete spaces is described by a system of first-order differential equations which can be formally written in the following fashion:

$$\frac{df_k}{dt} = -\mathbf{A} f_k, \tag{1}$$

where f_k is a N-dimensional vector with the values given at each node k and $\mathbf{A}$ is the discrete version of the Laplacian operator.

First, we consider the classical formula derived by the incremental ratio method, thus the matrix $\mathbf{A}$, also known as the adjacency matrix, denoted as $\mathbf{A_1}$ in the introduction, is such that the diagonal elements are $(A_1)_{kk} = 2$ for $k = 1, \ldots, N$ and the non-diagonal elements are $(A_1)_{kj} = -1$ if $k = j \pm 1$ and $(A_1)_{kj} = 0$ otherwise. For this problem, the eigenvectors and the eigenvalues are known from literature [16] and equal

$$\begin{aligned} q_k(n) &= \sin\left(n\frac{2k\pi}{N}\right) + \sin\left[(N-n)\frac{2k\pi}{N}\right] \\ &= 2\sin(k\pi)\cos\left[k\pi\frac{(N-2n)}{N}\right] \end{aligned} \tag{2}$$

and

$$\lambda_k = 2 - 2\cos\left(\frac{2k\pi}{N}\right) \quad \text{with} \quad k = 0, \ldots, N-1. \tag{3}$$

Now, we turn our attention to the second implemented method: the three-point formula. The diffusion equation can be written as

$$\frac{df(n)}{dt} = f_c''(n), \tag{4}$$

where the second-order derivative for node n, $f_c''(n)$, is given by (A11) of the Appendix. Inserting this equation into (4) one obtains

$$\begin{aligned} \frac{df(n)}{dt} &= \frac{1}{16}[f(n-4) + f(n+4)] \\ &\quad -\frac{1}{2}[f(n-3) + f(n+3)] \\ &\quad +[f(n-2) + f(n+2)] \\ &\quad +\frac{1}{2}[f(n-1) + f(n+1)] - \frac{17}{8}f(n). \end{aligned} \tag{5}$$

Knowing that the last equation should be written in a similar way as (1), we deduce that the Laplacian operator $\mathbf{A_3}$ has the following properties: $(A_3)_{ii} = \frac{17}{8}$, $(A_3)_{ii\pm1} = -\frac{1}{2}$, $(A_3)_{ii\pm2} = -1$, $(A_3)_{ii\pm3} = \frac{1}{2}$, and $(A_3)_{ii\pm4} = -\frac{1}{16}$. Thus, the three-point formula method considers interactions until fourth-order neighbor, different than the incremental ratio method, which consider only the nearest neighbors interaction. Now, we need to solve the eigenvalue problem for this new matrix $\mathbf{A_3}$ and to do this we follow the procedure applied with great success in Refs. [18, 20, 21, 33]. We consider the diffusion equation of a generical node n, given by (5).

One possible solution is written as

$$f(n) = \sum_k C_k q_k(n) \exp(-\lambda_k t), \tag{6}$$

where the C_k are n-independent constants, λ_k are the eigenvalues of the matrix $\mathbf{A_3}$ defined above, and $q_k(n)$ are its eigenfunctions. By inserting (6) into (5), one gets

$$\begin{aligned} \left(\frac{17}{8} - \lambda_k\right) q_k(n) &- \frac{1}{2}[q_k(n+1) + q_k(n-1)] \\ &- [q_k(n+2) + q_k(n-2)] + \frac{1}{2}[q_k(n+3) + q_k(n-3)] \\ &- \frac{1}{16}[q_k(n+4) + q_k(n-4)] = 0. \end{aligned} \tag{7}$$

One solution of the last equation is $\lambda_k = 0$, which corresponds to the totally symmetric eigenmode $q_k = const$ for all qs. The other solutions are obtained by observing that the functions $\tilde{q}_k(n) = \cos(n\psi_k)$ and $\tilde{\tilde{q}}_k(n) = \sin(n\psi_k)$ both fulfill (7) when the eigenvalues λ_k equal to

$$\lambda_k = \frac{17}{8} - \cos(\psi_k) - 2\cos(2\psi_k) + \cos(3\psi_k) - \frac{1}{8}\cos(4\psi_k). \tag{8}$$

We stop to mention that similar forms with this analytical expression for the eigenvalues have been also obtained for the energy bands (eigenvalues of the Hamiltonian and the overlap matrices) for 1D linear chain of atoms and for periodic lattices of atoms calculated using the tight-binding method [34, 35].

Now the eigenfunctions q_k can be expressed as linear combination of the two previous solutions, thus the eigenfunctions can be written as

$$q_k(n) = A \cdot \cos(n\psi_k) + B \cdot \sin(n\psi_k) \tag{9}$$

where the ψ_k and the constants A and B will be determined by making use of the periodic boundary conditions.

Here, for a ring, one should keep in mind that the first node ($n = 1$) has additionally a direct connection with the last node ($n = N$). Thus, the boundary condition makes that the equation corresponding to the first node, obtained from (7), to be given by:

$$\begin{aligned} \left(\frac{17}{8} - \lambda_k\right) q_k(1) &- \frac{1}{2}[q_k(2) + q_k(N)] - [q_k(3) + q_k(N-1)] \\ &+ \frac{1}{2}[q_k(4) + q_k(N-2)] - \frac{1}{16}[q_k(5) + q_k(N-3)] = 0. \end{aligned} \tag{10}$$

In a similar way, making use of the periodic boundary condition one can write for the last node ($n = N$):

$$\left(\frac{17}{8} - \lambda_k\right) q_k(N) - \frac{1}{2}[q_k(1) + q_k(N-1)] - [q_k(2) + q_k(N-2)] + \frac{1}{2}[q_k(3) + q_k(N-3)] - \frac{1}{16}[q_k(4) + q_k(N-4)] = 0. \quad (11)$$

We insert (8) and (9) into (10) and after some calculations we obtain the values of the eigenfunctions q_k:

$$\begin{aligned} q_k(n) = & -\frac{1}{16}\sin[(n-N+3)\psi_k] + \frac{1}{2}\sin[(n-N+2)\psi_k] \\ & - \sin[(n-N+1)\psi_k] - \frac{1}{2}\sin[(n-N)\psi_k] \\ & - \frac{1}{16}\sin[(n-5)\psi_k] + \frac{1}{2}\sin[(n-4)\psi_k] \\ & - \frac{17}{16}\sin[(n-3)\psi_k] - \frac{1}{2}\sin[(n-2)\psi_k] \\ & + \frac{1}{2}\sin(n\psi_k) + \sin[(n+1)\psi_k] - \sin[(n+2)\psi_k] \\ & - \sin[(n+3)\psi_k] + \frac{1}{2}\sin[(n+4)\psi_k] \\ & - \frac{1}{16}\sin[(n+5)\psi_k]. \end{aligned} \quad (12)$$

Now the eigenmodes given by (12) are inserted into the second boundary condition, (11), and we obtain the condition which ψ_k should fulfilled

$$\begin{aligned} & -\frac{9}{8}\sin\psi_k - \frac{63}{32}\sin(2\psi_k) - \frac{9}{16}\sin(3\psi_k) + \frac{23}{8}\sin(4\psi_k) \\ & - \frac{3}{16}\sin(5\psi_k) - \frac{27}{32}\sin(6\psi_k) + \frac{95}{256}\sin(7\psi_k) \\ & - \frac{1}{16}\sin(8\psi_k) + \frac{1}{256}\sin(9\psi_k) - \frac{1}{256} + \sin[(N-7)\psi_k] \\ & - \frac{15}{16}\sin[(N-6)\psi_k] - \frac{3}{8}\sin[(N-5)\psi_k] \\ & + \frac{29}{32}\sin[(N-4)\psi_k] + \frac{27}{16}\sin[(N-3)\psi_k] \\ & - \frac{465}{256}\sin[(N-1)\psi_k] + \frac{1}{16}\sin(N\psi_k) \\ & - \frac{41}{128}\sin[(N+1)\psi_k] + \frac{31}{32}\sin[(N+2)\psi_k] \\ & + \frac{1}{4}\sin[(N+3)\psi_k] - \frac{63}{32}\sin[(N+4)\psi_k] \\ & - \frac{3}{16}\sin[(N+5)\psi_k] + \frac{29}{32}\sin[(N+6)\psi_k] \\ & - \frac{3}{8}\sin[(N+7)\psi_k] + \frac{1}{16}\sin[(N+8)\psi_k] \\ & - \frac{1}{256}\sin[(N+9)\psi_k] = 0. \end{aligned} \quad (13)$$

The values of ψ_k which solve (13) are substituted in (8) and provide the eigenvalues of the matrix $\mathbf{A_3}$. In Fig. 1, we plot the eigenvalue spectrum of a small ring consisting of $N = 9$ nodes for the two methods: the incremental ratio and the three point formula. We represent with red squares the eigenvalues obtained by implementing the first method, (3), and with black circles the eigenvalues of the three point formula method given by (8) and (13). On the x-axis, we display the progressive number of the eigenvalues, namely from the lowest eigenvalue to the highest, while the y-axis corresponds to the eigenvalues. The highest eigenvalue is greater by employing the three-point formula method, while the lower non-zero eigenvalues are larger for incremental ratio method. One can notice that for both methods, the eigenvalues are twofold degenerated, except the first eigenvalue, $\lambda_k = 0$. In order to visualize the eigenmodes, we provide in Fig. 2 the eigenmodes for $N = 10$ for the three-point derivative method. These modes are the same for both methods, only their magnitudes and the corresponding eigenvalues are different. For instance, the last eigenmode in Fig. 2 corresponds to $\lambda \approx 2.58$, while for incremental ratio method corresponds to $\lambda \approx 1.38$. It is important to stress that the eigenvalue equal to zero is non-degenerated for odd values of N, while for even values of N the three-point formula gives two zero eigenvalues. For even values of N, the incremental ratio method provides only one vanishing eigenvalue, which corresponds to a situation where all the nodes move in the same direction (see the first drawing of Fig. 2). The second eigenmode shown in Fig. 2 corresponds to eigenvalue $\lambda_2 = 4.0$ for incremental ratio method and exceptionally gives another vanishing eigenvalue for three point formula method. All the other eigenvalues are double degenerated and correspond to the situation when some nodes are not moving.

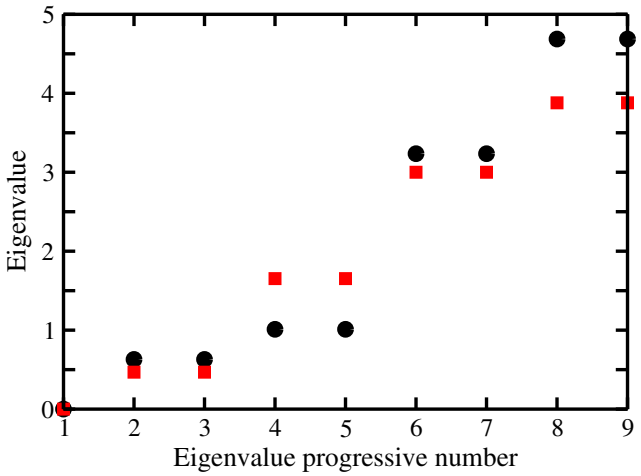

Fig. 1 Eigenvalue spectra of the Laplacian operator for a ring of $N = 9$ nodes. The *red squares* correspond to the values of incremental ratio method and the *black circles* correspond to the values of three point derivative method

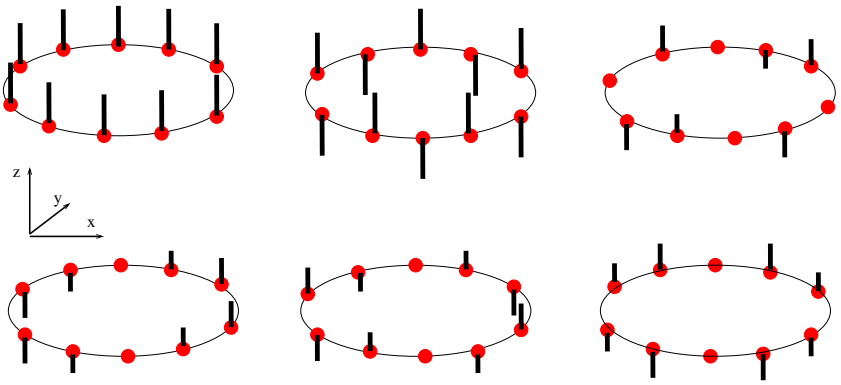

Fig. 2 Eigenmodes obtained by deploying the three-point formula method for a ring of $N = 10$ nodes. The eigenmodes corresponds to $\lambda_1 = 0.0$, $\lambda_2 = 0.0$, and $\lambda_3 \approx 4.82$ (first row from left to right) and $\lambda_5 \approx 0.49$, $\lambda_7 \approx 2.72$, and $\lambda_9 \approx 2.58$ (second row from left to right)

Let us consider now the eigenvalue spectra for larger structures. In Fig. 3, we plotted the spectrum of the matrix **A** for a ring of 10501 nodes obtained from implementing the two methods: the incremental ratio (solid red line) and the three-point derivative (solid black line). For a better comparison, we plot the eigenvalues in progressive order, namely from the lowest to the highest. One can easily notice that the eigenvalues of the connectivity matrix $\mathbf{A_1}$ range from 0 to 4. This result agrees with the theoretical prediction, (3), calculated in the limiting cases: $k = 0$ and $k = N - 1$, for large N. The eigenvalue spectrum of the matrix $\mathbf{A_3}$ has an up boundary equal to $\lambda_{\max} = \frac{9+6\sqrt{3}}{4}$. This value can be found by writing (8) only as a function of $\cos\psi_k$:

$$\lambda_k = 4 - 4\cos\psi_k - 3\cos^2\psi_k + 4\cos^3\psi_k - \cos^4\psi_k, \quad (14)$$

where we used some basic trigonometric transformations. Minimizing the last equation, we found out that the highest eigenvalue $\lambda_{\max}$ is reached for $\cos\psi_k = \frac{1-\sqrt{3}}{2}$.

Remarkably, the spectrum of $\mathbf{A_3}$ can be divided in two regions (except the two lowest eigenvalues): the first domain goes until the eigenvalue progressive number 6000 and here the eigenvalues are lower than those of $\mathbf{A_1}$, while in the second region (higher than 6000) the eigenvalues of $\mathbf{A_3}$ are higher. We stop to mention that similar results are obtained for any size N of the structure. This behavior has implications which will become clear in the next section.

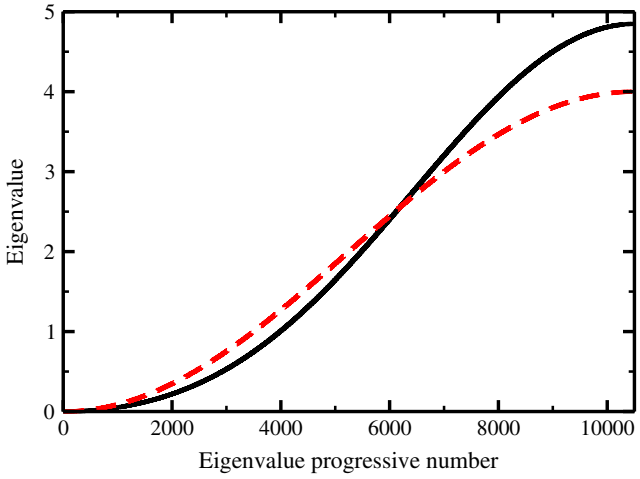

Fig. 3 Eigenvalue spectra of the Laplacian operator for a ring of $N = 10501$ nodes. The *red dashed line* corresponds to the values of incremental ratio method; the *black solid line* corresponds to the values of three point derivative method

3 Diffusion on Ring: Residual Concentration

As stressed in the first section, we focus on the diffusion on structures and from the wealth of applications we choose to study the behavior of the residual concentration at the initial node, $C(t)$. In this article, we consider that the diffusion of the particles occurs over structures which have a ring-shape topology. We stop to note that this problem is from the mathematical point of view strictly related to that of the energy transfer and trapping [36–38]. As we proceed to discuss, the residual concentration problem studied here admits a closed-form expression. Now, the residual concentration at the initial node obeys the master equation

$$\frac{dC_i(t)}{dt} = \sum_{j=1}^{N}{}' T_{ij} C_j(t) - \left(\sum_{j=1}^{N}{}' T_{ij}\right) C_i(t), \quad (15)$$

where $C_i(t)$ is the concentration at node i at time t, T_{ij} denotes the transfer rate from node j to node i, and the prime excludes the case $i = j$ from the sum. We assume that all the microscopic rates to nearest neighbors are equal, say k, and (15) becomes

$$\frac{dC_i(t)}{dt} = -k\sum_{j=1}^{N}{}' A_{ij} C_j(t) - kA_{ii}C_i(t), \quad (16)$$

where the elements A_{ij} correspond to matrix $\mathbf{A_1}$ for the incremental ratio method or to $\mathbf{A_3}$ for the three point formula. The last equation can be rewritten in a simple matrix form as

$$\frac{d}{dt}\mathbf{C}(t) = -k\mathbf{A}\mathbf{C}(t) \quad (17)$$

by introducing $\mathbf{C}(t) = (C_1(t), C_2(t), \ldots, C_N(t))^T$, where T denotes the transposed vector.

The matrix $\mathbf{A}$ is real and symmetric and can be diagonalized by using the following transformation

$$\Lambda = \mathbf{Q}^{-1}\mathbf{A}\mathbf{Q}, \tag{18}$$

where matrix $\mathbf{Q}$ consists of a complete, orthonormal set $\{\mathbf{q}_k\}$ of eigenvectors of $\mathbf{A}$, and $\mathbf{\Lambda}$ is a diagonal matrix which has on its diagonal the eigenvalues $\lambda_i (i = 1, \ldots, N)$. These eigenvalues are real and non negative, as noticed in Section 2.

Equation (17) is solved by using (18). One has namely, by setting $\mathbf{S}(t) = \mathbf{Q}^{-1}\mathbf{C}(t)$

$$\frac{d}{dt}\mathbf{S}(t) = \frac{d}{dt}\mathbf{Q}^{-1}\mathbf{C}(t) = -k\mathbf{Q}^{-1}\mathbf{A}\mathbf{Q}\mathbf{Q}^{-1}\mathbf{C}(t) = -k\Lambda\mathbf{S}(t), \tag{19}$$

which admits an immediate integration. In matrix form the solution reads

$$\mathbf{C}(t) = \mathbf{Q}\exp(-kt\mathbf{\Lambda})\mathbf{Q}^{-1}\mathbf{C}(0). \tag{20}$$

If all the particles are initially concentrated on node i, $C_j(0) = \delta_{ij}$, one has at later times the concentration at node n given by

$$C_n(t) = \sum_{m=1}^{N} Q_{nm}\exp(-kt\lambda_m)(\mathbf{Q}^{-1})_{mi}, \tag{21}$$

and the concentration of being at the initial site i is

$$C_i(t) = \sum_{m=1}^{N} Q_{im}(\mathbf{Q}^{-1})_{mi}\exp(-kt\lambda_m). \tag{22}$$

One notices that a considerable simplification occurs by averaging over all possible starting nodes

$$< C(t) > = \frac{1}{N}\sum_{i=1}^{N} C_i(t) = \frac{1}{N}\sum_{m=1}^{N}\left[\sum_{i=1}^{N}(\mathbf{Q}^{-1})_{mi}\,Q_{im}\right] \times \exp(-kt\lambda_m). \tag{23}$$

Knowing that $\mathbf{Q}^{-1}\mathbf{Q} = 1$, it follows that the residual concentration at the initial node is given by

$$< C(t) >= \frac{1}{N}\sum_{i=1}^{N}\exp(-kt\lambda_i), \tag{24}$$

an expression which depends on all the eigenvalues λ_i of the connectivity matrix $\mathbf{A}$, but not on the eigenvectors $\mathbf{Q}$. Remarkably, since all nodes in a ring are topologically equivalent, we deduce that $C_i(t) =< C(t) >$, see [39], and then

$$C_i(t) = \frac{1}{N}\sum_{i=1}^{N}\exp(-kt\lambda_i). \tag{25}$$

In other physical contexts, several forms similar to (24) have been established: fluorescence depolarization by quasiresonant energy transfer [20, 25, 36], the dynamics of polymer networks under free-draining conditions [18, 33, 40–42], the quantum mechanical problem of coherent exciton motion [43, 44]. In all these cases, the problem reduces to the determination of the full eigenvalue spectrum of the connectivity matrix $\mathbf{A_1}$. This task can be performed numerically, but as we mentioned in Section 1, there are some cases in which, by making use of the symmetries of the network, show an analytical solution [18–31].

We can now evaluate $< C(t) >$, (24), for very large structures. In this way, we obtain the residual concentration at the initial site after a time interval t. We set $k = 1$ and we display in Fig. 4 the concentration $< C(t) >$ for rings with $N = 10501$. The black solid line shows the results obtained by using the three point formula with the eigenvalues given by (8) and (13), the red dashed line denotes the results obtained from the incremental ratio method, with the eigenvalues given by (3). At long times, each curve ends in a plateau, because concentration gets to be equal to all the sites of the ring. In the long time limit, each site has the concentration equal to $1/N$. In the intermediate times region, for both curves, we observe power-law behavior and the values of the residual concentration obtained by the three point formula are larger than the ones achieved by the incremental ratio. The value of the slope obtained for both curves in the intermediate domain equals -0.5. This value was expected for the incremental ratio method [16, 45] due to the fact that the ring type structures as well the linear chains can be considered as the simplest fractals with the theoretical calculated spectral dimension $d_{st} = 1$. For the three point formula, where the interactions are taken into account up to the fourth nearest neighbor, the obtained value of the slope is a novelty. Formally, the existence of

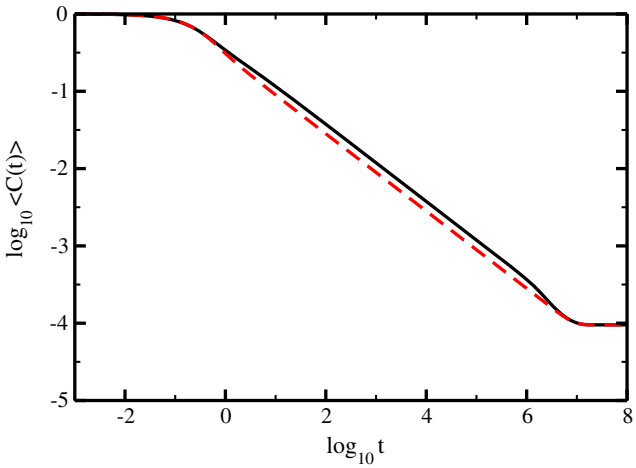

Fig. 4 Residual concentration at the starting node versus time. The *red dashed line* corresponds to the values of incremental ratio method; the *black solid line* corresponds to the values of three point derivative method. Both axes are in logarithmic scale to base 10

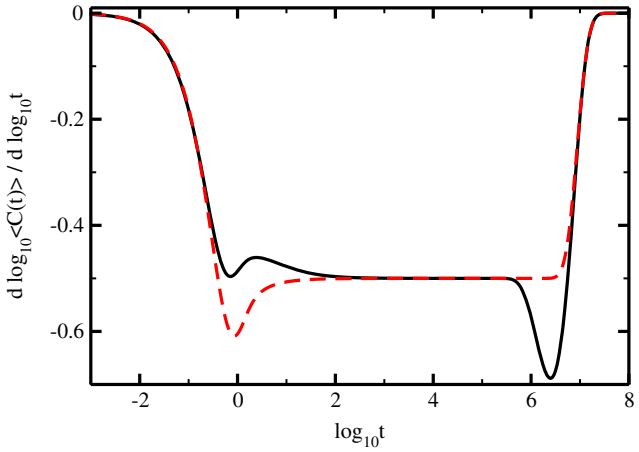

Fig. 5 Derivatives of the curves showed in Fig. 4. For derivatives, the same colors of the primitive curves were adopted. Both axes are in logarithmic scale to base 10

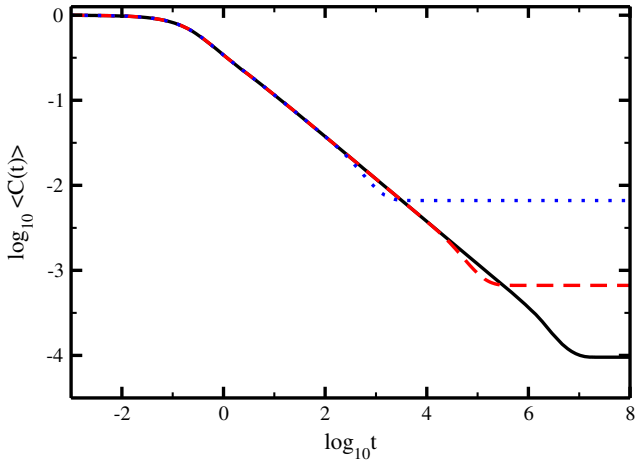

Fig. 6 Residual concentration at the starting node versus time starting from the $\mathbf{A_3}$ Laplacian operator (see the text for details). The *black solid line* corresponds to a ring with $N = 10501$; the *red dashed line* is for $N = 1501$ and the *blue dotted line* is obtained for a ring of $N = 151$

a scaling behavior means that $< C(t) >$ is well represented by a power-law $< C(t) > \propto t^{-0.5}$, the value of the power-law exponent being related to the spectral dimension, i.e. $d_{st}/2$. For a better visualization of the differences between the two methods, we plot in Fig. 5 the derivatives $\frac{d(log_{10}<C>)}{d(log_{10}t)}$ of the curves shown in Fig. 4. In the intermediate time region, immediately apparent is the constant slope of -0.5 for both curves. For $log_{10}t \approx 6.5$, the residual concentration $< C(t) >$ shows a minimum in the slope equal to -0.65, which was not observed for the incremental ratio method. For times $t \approx 1$, we notice for the first method a pronounced local minimum of slope equal to 0.6, which is transformed into a sequence of one local minimum and one maximum by implementing the three point formula.

In Fig. 6, we display in double logarithmical scale the residual concentration at the starting node for different sizes of the ring. Here, we focus on the rings with $N = 10501$ (solid black line), $N = 1501$ (red dashed line), and $N = 151$ (blue dotted line). We show only the results obtained from the three-point formula. Again, what is immediately clear is that in the intermediate time domain (which grows by increasing the size of the ring) the decay is linear in the chosen double logarithmical scale. The decay curves show at long times a plateau with its value equal to $1/N$, while for all curves is observed a kink right before reaching the equilibrium state.

4 Relaxation Patterns

Most measurements on polymers are not monitored in time but in frequency domain. Given the novel experimental methods by which parts of the polymer can be moved by optical tweezers and through attached magnetic beads, we are also interested in the mechanical relaxation. Under oscillatory shear, the response of the polymer system defines two moduli, the storage or elastic modulus $G'(\omega)$, and the loss or viscous modulus $G''(\omega)$. The two together make up the complex modulus which characterizes the mechanical relation response of the polymer over a large frequency range. For $\omega > 0$, these quantities are given by (see also Eq. 4.159 and 4.160 of Ref. [40]):

$$G'(\omega) = \frac{S}{N}\sum_{m=2}^{N}\frac{(\omega/2\sigma\lambda_i)^2}{1+(\omega/2\sigma\lambda_i)^2} \tag{26}$$

$$G''(\omega) = \frac{S}{N}\sum_{m=2}^{N}\frac{(\omega/2\sigma\lambda_i)}{1+(\omega/2\sigma\lambda_i)^2}. \tag{27}$$

For very dilute solutions, one has $S = \nu k_B T$, where ν is the number of polymer segments(beads) per unit volume. The λ_i are the eigenvalues. The vanishing eigenvalue (or eigenvalues for the three point formula case) are excluded from the sum. For concentrated solutions, when the entanglements effects are negligible, the two equations still hold, and only the value of S changes. We also note that the factor 2 in the expression $\omega/2\sigma\lambda_i$ arises from the second moment of the displacements involved in computing the stress required in the evaluation of the complex modulus.

Figures 7 and 8 present the results obtained for the mechanical relaxation moduli $G'(\omega)$ and $G''(\omega)$. We plot the (26) and (27) in dimensionless units, by setting $\sigma = 1$ and $S/N = 1$. In both figures, the ring size extends from $N = 5000$ to $N = 30,000$. The solid lines correspond to the results obtained with three point formula and the dashed lines represent the results achieved using the incremental ratio method. What appears immediately in

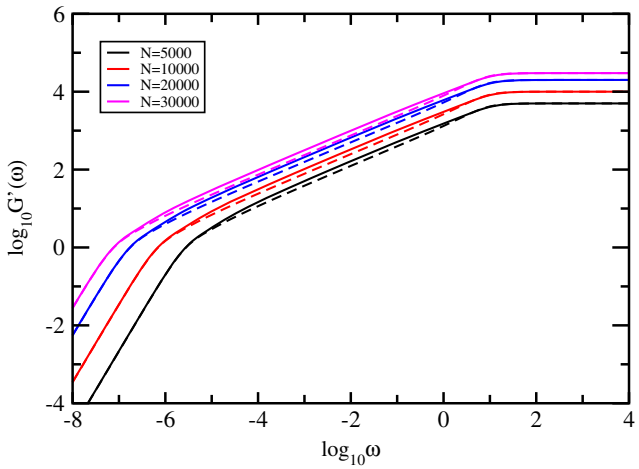

Fig. 7 The storage modulus for ring polymers. The *solid curves* show the results for three-point formula and the *dashed lines* correspond to incremental ratio method

the double logarithmic scales of the figures are the limiting, connectivity-independent behaviors at very small and very high frequencies; for $\omega \ll 1$ one has $G'(\omega) \sim \omega^2$ and $G''(\omega) \sim \omega$ and for $\omega \gg 1$ one finds $G'(\omega) \sim \omega^0$ and $G''(\omega) \sim \omega^{-1}$. Our main focus is again the region between the very small and very large frequencies; this in-between region appears for both mechanical relaxation moduli ($G'(\omega)$ and $G''(\omega)$) as a straight line and is again dominated by the value of the spectral dimension. In Fig. 7 for the three-point formula method, going from $N = 5000$ to $N = 30000$, we have a change in the slope from 0.505 to 0.501 and for the incremental ratio method the change is from 0.517 to 0.506. In the same manner, in Fig. 8 for the three point formula method, going from $N = 5000$ to $N = 30000$ we have a change in the slope from 0.478

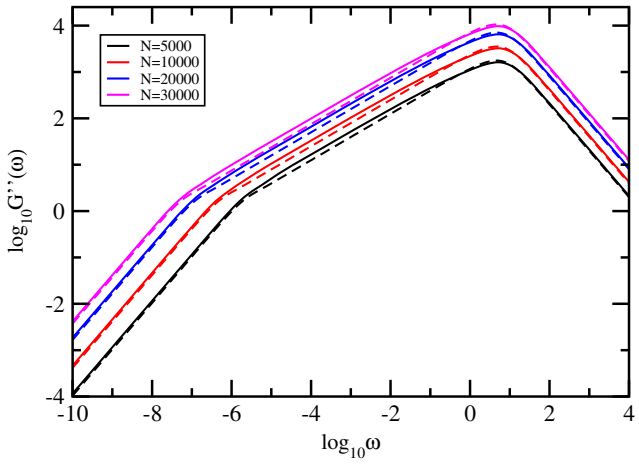

Fig. 8 The loss modulus for ring polymers. The *solid curves* show the results for three-point formula and the *dashed lines* correspond to incremental ratio method

to 0.488 and for the incremental ratio method the variation is from 0.498 to 0.499. From the comparation of these values with the theoretical expected $d_{st}/2 = 0.5$ results a very good accuracy. We find systematically lower values for the slopes of $G''(\omega)$ than for $G'(\omega)$. This is absolutely in line with our findings in other systems, such as dual Sierpinski gaskets [24], Vicsek fractals [26, 27], and multihierarchical structures [28]. If for the incremental ratio method this power-law behavior and the exponent value was expected, for the three-point formula method, the obtained results are a novelty. They show that even if the interactions are taken up to the fourth nearest neighbor, the solely exponent of importance for the mechanical relaxation is the spectral dimension and the geometry of the structure is very well reflected by its dynamical behavior. Also, we observe significant quantitative differences between the two methods. In the intermediate frequency domain, for the same N, the values of $G'(\omega)$ and $G''(\omega)$ obtained by using the three-point formula method are larger than the ones achieved by using the incremental ratio method. This difference increases by increasing the value of N; as one can see from both figures, the values of $G'(\omega)$ and $G''(\omega)$ obtained for $N = 30000$ by using the incremental ratio are almost similar with the ones obtained for $N = 20000$ by using the three-point formula.

5 Radius of Gyration

A basic structural feature of a polymer structure is its radius of gyration. It is a measure of the size of the molecule. Here, practically, we want to see if the consideration of the interactions between more distant neighbors will affect the scaling behavior of the mean squared radius of gyration and also its values. In the framework of GGS model, the refs. [46–48] have obtained for the mean squared radius of gyration, in the free-draining case, an expression which depends only on the eigenvalues of the discrete version of the Laplacian operator. It reads as

$$< R_g^2 >= \frac{l}{N} \sum_{i=2}^{N} \frac{1}{\lambda_i}, \tag{28}$$

where λ_i are the eigenvalues of the discrete version of the Laplacian operator $\mathbf{A}$, l is the averaged length of an isolated bond in thermal equilibrium, and N is the total number of nodes in the structure or, equivalently the size of the structure. The vanishing eigenvalue $\lambda_1 = 0$ is not taken into account, the sum in (28) runs from the smallest positive eigenvalue λ_2, connected with the extension and topology of the structure, to the largest eigenvalue λ_N, determined by the entropic spring constant and by the maximal number of nearest neighbors of a bead.

For fractal objects with spectral dimension less than 2, the smallest eigenvalue, $\lambda_{\min}$, is inversely proportional to the time, t, needed by a random walker to explore the whole structure of size N. Using the Zimm-Stockmayer relation [49] $N \sim t^{d_s/2}$, where d_s denotes the spectral dimension of the structure, one obtains

$$\lambda_{\min} \sim t^{-1} \sim N^{-2/d_s}. \tag{29}$$

Inserting (29) into (28) one gets for fractals with $d_s < 2$

$$< R_g^2 > \sim \lambda_{\min}^{(d_s-2)/2}. \tag{30}$$

Now, combining (29) and (30), the mean squared radius of gyration reads

$$< R_g^2 > \sim N^{\frac{2-d_s}{d_s}}. \tag{31}$$

The scaling relation of the mean averaged radius of gyration from (31) is identical to the one obtained by Cates [50].

Figure 9 shows the results for the mean squared radius of gyration, given by (28) in which we set $l = 1$. The black line corresponds to the mean squared radius of gyration obtained using the three-point formula with the eigenvalues given by (8) and (13), respectively, the red dashed line corresponds to the mean squared radius of gyration determined by using the incremental ratio method with the eigenvalues given by (3). In the figure, for both methods, we use rings ranging from $N = 10$ to $N = 10000$. For rings with small sizes, up to $N = 30$, the values of $< R_g^2 >$ determined with both methods are very akin. Then, increasing N, we systematically obtain that the values of $< R_g^2 >$ calculated using the three-point formula are larger than the ones of $< R_g^2 >$ calculated with the incremental ratio. In Fig. 9, both curves appear as straight lines which clearly denote power-law behavior. In the region extending from $N = 100$ to $N = 10000$, we find that the value of the slope is 1.003 for $< R_g^2 >$ determined by using the three-point formula and 1.000 for $< R_g^2 >$ obtained by the incremental ratio method. Equaling the exponent of (31) with the value of the slope, we determine the spectral dimension to be $d_s = 0.998$ for three-point formula and $d_s = 1.000$ for incremental ratio method. The agreement with the theoretical expected value $d_{st} = 1$ is excellent for both methods.

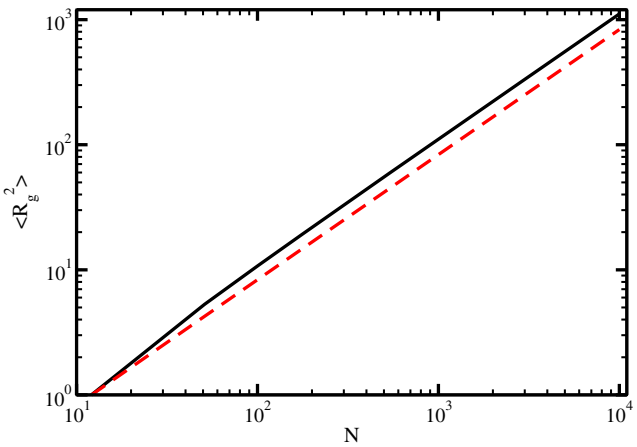

Fig. 9 Mean squared radius of gyration for ring polymers. The *solid black curve* shows the results for three-point formula and the *dashed line* corresponds to the incremental ratio method

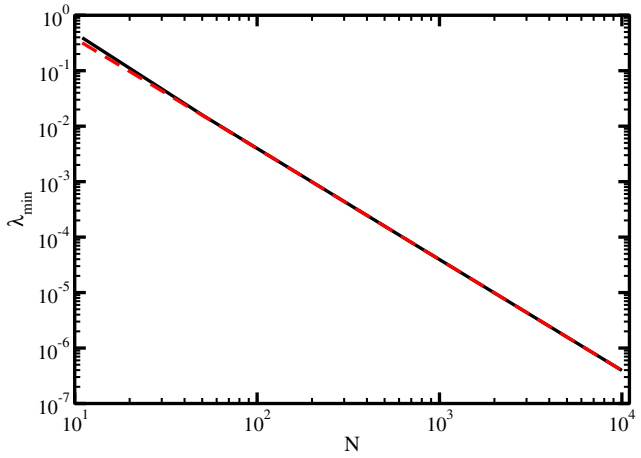

Fig. 10 The smallest eigenvalue for ring polymers. The *solid black curve* shows the results for three point formula and the *dashed line* corresponds to incremental ratio method

Figure 10 displays the behaviors of the smallest eigenvalue of the matrix $\mathbf{A_3}$ (black line) and of the matrix $\mathbf{A_1}$ (red dashed line). The number of nodes in the ring extends from $N = 10$ to $N = 10000$ and the scales of the figure are double-logarithmic to base 10. For rings with small sizes, up to $N = 30$, the smallest eigenvalue of the $\mathbf{A_3}$ is a little bit larger than the smallest eigenvalue of the $\mathbf{A_1}$. Then, increasing the size of the ring, both smallest eigenvalues of $\mathbf{A_3}$ and respectively $\mathbf{A_1}$ have almost similar values and the curves overlap. In the double-logarithmic scales of Fig. 10, the curves are very smooth, fact which does suggest the scaling. Linear approximations in the region $N = 100$ to $N = 10000$ lead for both curves to the same value of the slope, -2. Equaling the scaling exponent of (29) with the obtained value of the slope, we find for the spectral dimension a value, $d_s = 1$. Again, the accuracy is excellent when comparing with the theoretical expected value $d_{st} = 1$.

6 Conclusions

In summary, in this work, we studied the relaxation dynamics and the diffusion on rings by means of the finite volume approximation to convert the continuum space into a system consisting of N nodes. By making use of the three-point formula, we generalized the connectivity matrix to incorporate interactions up to the fourth nearest neighbor of a monomer.

For this new Laplacian matrix, we developed an iterative procedure for the determination of its eigenvalue spectrum. Based on the eigenvalues obtained iteratively, we analyzed the relaxation dynamics by investigating the behavior of the mechanical relaxation moduli and the diffusion process by focusing on the behavior of the normalized residual concentration at the initial node. We compared our results with the ones achieved by using the incremental ratio method. The eigenvalue spectra of the two methods are quite different except the vanishing eigenvalue and to the fact that all the other eigenvalues are twofold degenerate. Despite the spectral differences, both techniques present common features at short and long times (or frequencies). Using the three-point formula method, we have showed that even if the interactions are taken up to the fourth nearest neighbor the solely exponent of importance for the relaxation dynamics is the spectral dimension and thus the geometry of the structure is very well reflected by its dynamical behavior. Also, in the intermediate frequency domain, the values of the mechanical relaxation moduli calculated by using the three-point formula are considerably larger than the ones determined by using the incremental ratio method.

The intermediate time range shows a negative exponential decay with exponent equal to -0.5, as expected by a standard Gaussian diffusion. Remarkably, diffusion simulated through the three-point formula, which is related to a better approximation, shows a higher concentration in the intermediate time region. We can conclude that by measuring the concentration at the initial node with the use of the incremental ratio, we underestimate its value. This result can have big relevance in experiments which require high precision degree. Using the two techniques, we also studied the behaviors of the mean squared radius of gyration of the rings and of the smallest eigenvalue of the Laplacian operator. From the analysis of the behaviors of the mean squared radius of gyration and of the smallest eigenvalue emerges clearly that the scaling relations are very well preserved by the introduction of interactions between more distant neighbors, based on three point formula method.

Acknowledgments M.G. acknowledges the financial support of the CNPq. A. J. thanks to Prof. Dr. Jens Uwe Sommer and to Dr. Michael Lang for many fruitful discussions.

Appendix A: Three-Point Formula Method for Derivatives

The three-point formula is a computational good alternative to the incremental ratio method when a calculation of the derivatives of a function is required. To overcome the problem of the truncation error, more evaluation points should be used. To generalize the approximation formulas for derivatives, a generalization of the Lagrange polynomials is developed. Instead of using only two points (x_0 and x_1) to define a Lagrange polynomial $f(x)$, a set of $n+1$ distinct numbers $x_0, x_1, x_2, ..., x_n$ is used:

$$f(x) = \sum_{k=0}^{n} f(x_k)L_k(x) + \frac{(x-x_0)\cdot\cdots\cdot(x-x_n)}{(n+1)!} f^{n+1}(\xi(x)), \tag{A1}$$

for a generic function $\psi(x)$ in the interval (x_0, x_n), where $L_k(x)$ is the $k-th$ Lagrange coefficient. Differentiating (A1) leads to:

$$\begin{aligned} f'(x) = &\sum_{k=0}^{n} f(x_k)L_k'(x) + D_x\left[\frac{(x-x_0)\cdot\cdots\cdot(x-x_n)}{(n+1)!}\right] \\ &\times f^{n+1}(\xi(x)) + \frac{(x-x_0)\cdot\cdots\cdot(x-x_n)}{(n+1)!} \\ &\times D_x\left[f^{n+1}(\xi(x))\right], \end{aligned} \tag{A2}$$

where $D_x[]$ is the derivative with respect to x.

This generalization is referred as (n+1)-point formula. For futher details about this derivation and the treatment of the error term, see [32]. Usually, higher is the number of evaluation points greater the accuracy will be. However, truncation error issues and expensive computational time lead to the use of three or five points formulas. In the present work, we focus on the three-points formula. Its derivation begins with the definition of the three Lagrange coefficients and their derivatives:

$$L_0(x) = \frac{(x-x_1)(x-x_2)}{(x_0-x_1)(x_0-x_2)} \quad L_0'(x) = \frac{2x-x_1-x_2}{(x_0-x_1)(x_0-x_2)} \tag{A3}$$

$$L_1(x) = \frac{(x-x_2)(x-x_0)}{(x_1-x_2)(x_1-x_0)} \quad L_1'(x) = \frac{2x-x_0-x_2}{(x_1-x_0)(x_1-x_2)} \tag{A4}$$

$$L_2(x) = \frac{(x-x_1)(x-x_0)}{(x_2-x_1)(x_2-x_0)} \quad L_2'(x) = \frac{2x-x_0-x_1}{(x_2-x_0)(x_2-x_1)}. \tag{A5}$$

Substituting (A3), (A4), and (A5) in (A2), we obtain after some manipulations the derivative of f

$$f'(x) = f(x_0)L_0'(x) + f(x_1)L_1'(x) + f(x_2)L_2'(x). \tag{A6}$$

If we consider $x_i = x_0 + ih$ and $h > 0$, we obtain the so-called forward derivative. We identify the point $x_i = x_0 + ih$ with node $n+i$, with i being any integer variable; thus node n corresponds to x_0. For simplicity, we choose $h = 1$.

Choosing $x = x_0$ (or node n) and inserting the values of L'_0, L'_1, and L'_2 into the last equation, we obtain the equation for the forward derivative:

$$f'_{for}(n) = -\frac{3}{2}f(n) + 2f(n+1) - \frac{1}{2}f(n+2). \quad \text{(A7)}$$

Similarly, the expression of the backward derivative is obtained by choosing $x = x_2$ and substituting in (A6), we get after some algebraic calculations

$$f'_{back}(n+2) = \frac{1}{2}f(n) - 2f(n+1) + \frac{3}{2}f(n+2). \quad \text{(A8)}$$

Renoting $n+2$ with n this equation can be rewritten as

$$f'_{back}(n) = \frac{3}{2}f(n) - 2f(n-1) + \frac{1}{2}f(n-2). \quad \text{(A9)}$$

We can average the $f'_{for}(n)$ and $f'_{back}(n)$ in order to have the centered derivative

$$f'_c(n) = \frac{1}{2}[f'_{for}(n) + f'_{back}(n)] = \frac{1}{4}f(n-2) - f(n-1) + f(n+1) - \frac{1}{4}f(n+2). \quad \text{(A10)}$$

Following the same procedure, we find an equivalent expression for the second derivative, i.e.,

$$f''_c(n) = \frac{1}{16}f(n-4) - \frac{1}{2}f(n-3) + f(n-2) + \frac{1}{2}f(n-1) - \frac{17}{8}f(n) + \frac{1}{2}f(n+1) + f(n+2) - \frac{1}{2}f(n-3) + \frac{1}{16}f(n+4). \quad \text{(A11)}$$

References

1. I.M. Sokolov, J. Klafter, Chaos **15**, 026103 (2005)
2. N.G. van Kampen. *Stochastic Processes in Physics and Chemistry* (North-Holland Amsterdam, 1992)
3. E. Scalas, R. Gorenflo, F. Mainardi, Phys. A **284**, 376 (2000)
4. E. Agliari, A. Blumen, O. Mülken, J. Phys. A **41**, 445301 (2008)
5. A.J. Martinez, M.I. Molina, J. Phys. A **45**, 275204 (2012)
6. E.W. Montroll, G.H. Weiss, J. Math. Phys. **6**, 167 (1965)
7. H. Scher, M. Lax, Phys. Rev. B **7**, 4491 (1973)
8. A. Jurjiu, T. Koslowski, C. von Ferber, A. Blumen, Chem. Phys. **294**, 187 (2003)
9. F. Hermeline, J. Comp. Phys. **160**, 481 (2000)
10. M. Bittelli, F. Tomei, A. Pistocchi, M. Flury, J. Bolle, E.S. Brooks, G. Antolini, Adv. Water Res. **33**, 106 (2010)
11. E. Heilbronner, H. Beck, *Das HMO-Modell und seine Anwendung*, vol. 1 (Weinheim: Chemie, 1968)
12. J.-U. Sommer, M. Schulz, H. Trautenberg, J. Chem. Phys. **98**, 7515 (1993)
13. J.-U. Sommer, T.A. Vilgis, G. Heinrich, J. Chem. Phys. **100**, 9181 (1994)
14. P. Biswas, R. Kant, A. Blumen, J. Chem. Phys. **114**, 2430 (2001)
15. A. Jurjiu, R. Dockhorn, O. Mironova, J.-U. Sommer, Soft Matter **10**, 4935 (2014)
16. P.E. Rouse, J. Chem. Phys. **21**, 1272 (1953)
17. A.A. Gurtovenko, A. Blumen, Adv. Polym. Sci. **182**, 171 (2005)
18. C. Cai, Z. Chen, Macromolecules **30**, 5104 (1997)
19. Z.Y. Chen, C. Cai, Macromolecules **32**, 5423 (1999)
20. M. Galiceanu, A. Blumen, J. Chem. Phys. **127**, 134904 (2007)
21. M. Galiceanu, J. Phys. A **43**, 305002 (2007)
22. M.G. Cosenza, R. Kapral, Phys. Rev. A **46**, 1850 (1992)
23. R. Rammall, J. Phys. **45**, 191 (1984)
24. A. Jurjiu, C. Friedrich, A. Blumen, Chem. Phys. **284**, 221 (2002)
25. A. Blumen, A. Volta, A. Jurjiu, T. Koslowski, Phys. A **356**, 12 (2005)
26. A. Blumen, C. von Ferber, A. Jurjiu, T. Koslowski, Macromolecules **37**, 638 (2004)
27. A. Blumen, A. Jurjiu, T. Koslowski, C. von Ferber, Phys. Rev. E **67**, 061103 (2003)
28. A. Jurjiu, A. Volta, T. Beu, Phys. Rev. E **84**, 011801 (2011)
29. A. Volta, M. Galiceanu, A. Jurjiu, T. Gallo, L. Gualandri, Mod. Phys. Lett. B **26**, 1250055 (2012)
30. H. Liu, Z. Zhang, J. Chem. Phys. **138**, 114904 (2013)
31. Z. Zhang, X. Guo, Y. Lin, Phys. Rev. E **90**, 022816 (2014)
32. R.L. Burden, J.D. Faires, *Numerical Analysis* (Brooks/Cole Publishing Group, New York, 1997), Sixth Edition
33. A.A. Gurtovenko, D.A. Markelov, Yu.Ya. Gotlib, A. Gotlib, J. Chem. Phys. **119**, 7579 (2003)
34. D.A. Papaconstantopoulos, *Handbook of the Band Structure of Elemental Solids* (Plenum Press, New York, 1986)
35. D.A. Papaconstantopoulos, M.J. Mehl, S.C. Erwin, M.R. Pederson, Mat. Res. Soc. Symp. Proc. **491**, 221 (1998)
36. A. Blumen, A. Volta, A. Jurjiu, T. Koslowski, J. Lumin. **111**, 327 (2005)
37. R. Kopelman, M. Shortreed, Z.Y. Shi, W. Tan, Z. Xu, J.S. Moore, A. Bar-Haim, J. Klafter, Phys. Rev. Lett. **78**, 1239 (1997)
38. A. Bar-Haim, J. Klafter, J. Phys. Chem. B **102**, 1662 (1998)
39. A. Volta, O. Mülken, A. Blumen, J. Phys. A **39**, 17997 (2006)
40. M. Doi, S.R. Edwards, *The Theory of Polymer Dynamics* (Clarendon, Oxford, 1986)
41. A.Yu. Grosberg, A.R. Khokhlov, *Statistical Physics of Macromolecules* (AIP, New York, 1994)
42. A. Volta, M. Galiceanu, A. Jurjiu, J. Phys. A: Math. Theor. **43**, 105205 (2010)
43. V.M. Kenkre, P. Reineker, *Exciton Dynamics in Molecular Crystals and Aggregates* (Springer, Berlin, 1982)
44. A. Blumen, V. Bierbaum, O. Mülken, Phys. A **371**, 10 (2006)
45. S. Alexander, R. Orbach, J. Phys. Lett. (Paris) **43**, L265 (1982)
46. J.-U. Sommer, A. Blumen, J. Phys. A **28**, 6669 (1995)
47. J.E. Martin, B.E. Eichinger, J. Chem. Phys. **69**, 4588 (1978)
48. B.E. Eichinger, J.E. Martin, J. Chem. Phys. **69**, 4595 (1978)
49. B.H. Zimm, W.H. Stockmayer, J. Chem. Phys. **17**, 1301 (1949)
50. M.E. Cates, Phys. Rev. Lett. **53**, 926 (1984)